IOP Publishing J. Phys. Mater. 7 (2024) 035005 https://doi.org/10.1088/2515-7639/ad558b

Journal of Physics: Materials

OPEN ACCESS

RECEIVED
30 October 2023

REVISED
20 May 2024

ACCEPTED FOR PUBLICATION
7 June 2024

PUBLISHED
20 June 2024

PAPER

Spin wave excitations in low dimensional systems with large magnetic anisotropy

Fernando Delgado[1,*], **Mikhail M Otrokov**[2,3,4,6] **and Andrés Arnau**[2,3,5]

[1] Instituto de estudios avanzados IUDEA, Departamento de Física, Universidad de La Laguna, C/Astrofísico Francisco Sánchez, s/n., La Laguna 38203, Spain
[2] Centro de Física de Materiales CFM/MPC (CSIC-UPV/EHU), Paseo Manuel de Lardizábal 5, 20018 Donostia-San Sebastián, Spain
[3] Donostia International Physics Center, Paseo Manuel de Lardizábal 4, 20018 Donostia-San Sebastián, Spain
[4] IKERBASQUE, Basque Foundation for Science, E-48011 Bilbao, Spain
[5] Departamento de Polímeros y Materiales Avanzados: Física, Química y Tecnología, Facultad de Química UPV/EHU, Apartado 1072, 20080 Donostia-San Sebastián, Spain
[6] Present address: Instituto de Nanociencia y Materiales de Aragón (INMA), CSIC-Universidad de Zaragoza, Zaragoza 50009, Spain.
[*] Author to whom any correspondence should be addressed.

E-mail: fdelgadoa@ull.edu.es

Keywords: magnons, spin waves, two-dimensional materials, ferromagnets, anisotropy

Supplementary material for this article is available online

Abstract

The low-energy excitation spectrum of a two-dimensional ferromagnetic material is dominated by single-magnon excitations that show a gapless parabolic dispersion relation with the spin wave vector. This occurs as long as magnetic anisotropy and anisotropic exchange are negligible compared to isotropic exchange. However, to maintain magnetic order at finite temperatures in extended systems, it is necessary to have sizable anisotropy to open a gap in the spin wave excitation spectrum. We consider four real two-dimensional systems for which ferromagnetic order at finite temperature has been observed or predicted. Density functional theory calculations of the total energy differences for different spin configurations permit us to extract the relevant parameters and connect them with a spin Hamiltonian. The corresponding values of the Curie temperature are estimated using a simple model and found to be mostly determined by the value of the isotropic exchange. The exchange and anisotropy parameters are used in a toy model of finite-size periodic chains to study the low-energy excitation spectrum, including single-magnon and two-magnon excitations. At low energies, we find that single-magnon excitations appear in the spectrum together with two-magnon excitations. These excitations present a gap that grows particularly for large values of the magnetic anisotropy or anisotropic exchange, relative to the isotropic exchange.

1. Introduction

The appearance of long-range ferromagnetic order at finite temperatures in unconfined two-dimensional systems requires the existence of magnetic anisotropy [1], so that a gap appears in the magnon (spin wave) excitation spectrum. Indeed, the magnitude of this gap is determinant for the Curie temperature T_C that marks the quenching of ferromagnetism. T_C also depends on the exchange coupling between spins, the magnitude of the spins, and the number of nearest neighbours [2]. In the case of localized spins at the atomic sites, e.g. in insulating systems, one typically uses a Heisenberg-like spin Hamiltonian that includes, at least, nearest neighbours isotropic exchange interactions between sites, as well as the single-ion anisotropy at each site and, additionally, anisotropic exchange or even antisymmetric exchange [3]. Single-ion anisotropy is determined by the crystal field around the magnetic atoms and the strength of spin-orbit interaction, this latter being also relevant for the anisotropic exchange. However, explaining the particular type of exchange interactions for each and every system is far from trivial and different models have been proposed [4].

From the experimental side, there are a bunch of experimental techniques that can be used to explore the magnetic order of thin films with magnetic anisotropy and, thus, the signatures of both single and

multi-magnon processes. This includes x-ray magnetic circular dichroism [5] and its depth-resolved variants [6, 7], neutron scattering, which has the additional advantage of direct access to the dispersion relation on the whole wave vector space [8, 9], magnetometry using SQUID [10], Raman spectroscopy [11–14], ferromagnetic resonance (FMR) [15–17] or local techniques, such as spin-polarized scanning tunneling microscopy [18] and inelastic tunneling spectroscopy [19–21]. Interestingly, only recently the effect of magnons in atomically thin layers has been accessible experimentally through Raman scattering [22], allowing for instance to determine the optical selection rules established by the interplay between crystal symmetry, layer number, and magnetic states in CrI_3. The case of magnon excitations in monolayer and bilayer CrI_3 has been also addressed in other studies [23–26].

Nowadays, the use of first-principles calculations permits obtaining accurate total energy values for different spin configurations of a given magnetic system. A proper choice of these configurations with different spin orientations allows fitting parameters defined in the spin Hamiltonian by mapping total energy differences, although with some limitations [27]. In this work, we have considered four two-dimensional systems of different kinds: (1) single septuple layer of the magnetic topological insulator $MnBi_2Te_4$, (2) single triple layer of a Mott-Hund's magnetic insulator CrI_3, (3) 2D metal-organic coordination network Fe-DCA on the Au(111) substrate, and (4) monolayer of Co on the heavy metal substrate Pt(111). The four systems have been shown [28–32] to present ferromagnetic order at finite temperatures and, therefore, are interesting to consider. Our aim here is to understand the nature and origin of the anisotropy [33, 34], as well as the spin wave excitation spectrum and Curie temperatures. In order to achieve a qualitative understanding, we use an auxiliary toy model of finite ferromagnetic spin chains with exchange and anisotropy parameters extracted from the previous mapping of the spin Hamiltonian.

2. Density functional theory (DFT) calculations and mapping to spin Hamiltonian

In this section we briefly describe the way DFT calculations have been performed for the four magnetic systems of interest, as well as the extraction of the exchange and anisotropy parameters that are later on used to model the spin wave excitations.

DFT calculations were performed using the projector augmented-wave method [35], implemented in the VASP code [36–38]. The generalized gradient approximation (GGA) was employed to describe the exchange-correlation energy [39]. To take into account the strongly localized character of the 3*d*-states (except those of Co in the Co/Pt system, which is metallic), we resorted to the GGA + U approach [40]. The $U_{\text{eff}} = U - \mathcal{J}$ [41] parameter was chosen to be equal to 2, 6, and 5.34 eV for Cr, Fe, and Mn 3*d*-states, respectively, following the literature [29, 31, 33]. For each system of interest, the atomic coordinates were relaxed using a force tolerance criterion for convergence of 0.01 eV $Å^{-1}$.

The calculations were performed in a model of repeating films separated by a vacuum gap of a minimum of 10 Å. According to test calculations, choosing thicker vacuum layer only affects the results marginally. In the Co/Pt and $MnBi_2Te_4$ systems [CrI_3 and Fe-DCA/Au(111) systems], in which the 3*d*-atom layer has a hexagonal [honeycomb] lattice, the $(1 \times \sqrt{3})$ [(1×1)] *magnetic* periodicity was used, so that the unit cell contains two *magnetic* atoms in each case (see figures 1(b) and (a), respectively).

The values of the nearest-neighbor Heisenberg exchange coupling constants J, anisotropic exchange λ [$(J^z - J)$ in table 1], and single-ion anisotropy D parameters (see equation (1) below where the spin Hamiltonian is explicitly given) were obtained via accurate static total-energy calculations, performed for the optimized crystal structures. While J is obtained via a scalar relativistic DFT calculation of ferromagnetic and antiferromagnetic configurations, determining λ and D requires (i) inclusion of spin–orbit coupling and (ii) consideration of the latter two magnetic configurations for both in-plane and out-of-plane moment directions. In all of these static total-energy calculations we used a strict convergence criterion of 10^{-8} eV, the $\overline{\Gamma}$-centered k-points sampling of the 2D Brillouin zone, and the tetrahedron integration method with Blöchl corrections. The specific Brillouin zone samplings are given in the supplementary information.

For the systems with a honeycomb lattice (Cr and Fe-containing systems), there are two magnetic atoms in the surface unit cell, and each atom is coordinated with three nearest neighbors (figure 1(a)). These three nearest neighbours can have ferromagnetic or antiferromagnetic coupling between them, with a magnetic interaction energy of $-3JS^2$ and $+3JS^2$ respectively, where S is the spin of each magnetic atom, which translates into a total energy difference of $6JS^2$.

For Co/Pt(111) and $MnBi_2Te_4$, the coordination of Co and Mn atoms is six and we have to use a $(1 \times \sqrt{3})$ unit cell that contains two magnetic atoms. For the cell shown in figure 1(b), the ferromagnetic coupling includes the six equal $-JS^2$ contributions, i.e. a total of $-6JS^2$, while the antiferromagnetic coupling includes two spins coupled ferromagnetically and four spins coupled antiferromagnetically, i.e. a total of $2JS^2$, which translates into a total energy difference of $8JS^2$. This number of aligned or antialigned spin pairs

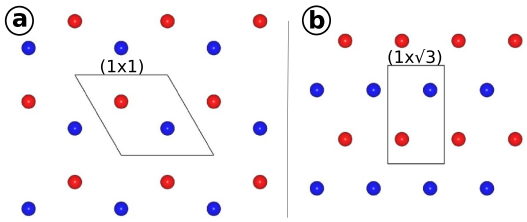

Figure 1. Top view of the two-dimensional structures of the systems considered (only magnetic atoms are drawn) showing the unit cells used in the calculations for the (1×1) honeycomb (a) and $(1 \times \sqrt{3})$ hexagonal (b) layer cases, both containing two atoms in the unit cell, the latter being actually a rectangular cell. The blue and red colors represent opposite spins in an antiferromagnetic configuration to illustrate the number of first neighbours with aligned and anti-aligned spins for each lattice: three anti-aligned spins in the honeycomb (a), while four anti-aligned and two aligned spins in the hexagonal (b). Notice that in a ferromagnetic configuration of spins the number of first neighbours with aligned spins coincides with the coordination, i.e, three in the honeycomb and six in the hexagonal lattice.

Table 1. 2D systems under study with the spin S of each magnetic atom (within brackets), the corresponding values of exchange couplings J, axial anisotropy D and anisotropic exchange $\lambda = J_z - J$ as extracted from DFT according to the mapping with Hamiltonian (1). T_C was calculated using the expressions provided in [42].

				T_C	
System	J (meV)	D (meV)	λ (meV)	$k_B T_C$(meV)	T_C(K)
Co/Pt ($S = 1$)	55.0	1.20	−0.11	26.9	312
CrI_3 ($S = 3/2$)	3.75	0.039	+0.16	3.73	43.2
Fe-DCA/Au ($S = 2$)	0.72	0.19	−0.021	1.50	17.4
$MnBi_2Te_4$ ($S = 5/2$)	0.22	0.056	−0.0075	1.27	14.76

counting is the same for the anisotropic exchange contribution, while the single-ion anisotropy term includes only two magnetic atoms per cell.

The results obtained for the four systems under study are given in table 1. In all cases, the largest energy scale corresponds to the isotropic exchange strength, which can be as large as tens of meV in the Co/Pt case but of the order of meV, or even less, in the three other cases. The calculated values of the isotropic exchange coupling constants for CrI_3 ($J = 3.75$ meV), $MnBi_2Te_4$ ($J = 0.22$ meV) and Co/Pt(111) ($J = 55$ meV) compare reasonably well with the values calculated by other authors using different methods. For example, for CrI_3, employing the state-of-the-art TB2J method [43], a value of $J = 2.1$ meV was obtained [44], while the four-state mapping method led to $J = 4.6$ meV [27]. Using the force theorem, values for $MnBi_2Te_4$ [28] of $J = 0.32$ meV and for Co/Pt(111) [45] $J = 42.5$ meV have been obtained. As shown in the next section, the isotropic exchange is crucial to determine the Curie temperature. The anisotropic exchange λ is, at least, two orders of magnitude smaller than the isotropic exchange J. The single-ion anisotropy D is larger than the anisotropic exchange, except for CrI_3. The largest value of $D/J = 0.26$ corresponds to the case of $MnBi_2Te_4$. These variations in the anisotropic exchange and single-ion anisotropy, relative to the isotropic exchange, have consequences in the spin wave excitation spectrum that are discussed in section 4.3: they will induce an energy gap in the spin waves excitation spectra.

3. Critical temperatures

The magnetic susceptibility of a ferromagnet obeys Curie-Weiss law where, above a critical temperature T_C, it behaves essentially as a paramagnet with an enhanced susceptibility [46], while below it, the material can keep a finite magnetization in the absence of applied field. Thus, it is important to estimate reasonable T_C values for the different systems. Torelli and Olsen [42] proposed a simple parametric dependence of T_C on the model parameters for different two-dimensional materials based on fitting to classical Monte Carlo simulations. The proposed T_C reproduces both the critical temperature in the large magnetic anisotropy limit, and in the low anisotropy limit where the commonly used random phase approximation [46] fails. Table 1 shows the critical temperatures extracted for the four materials studied in section 2. Notice that since $D/J,\ \lambda/J \ll 1$ in all cases, the value of the critical temperature is essentially determined by the value of the isotropic exchange J, the number of nearest neighbours and the magnitude of the spin magnetic moment S [42]. However, it requires finite values of the anisotropy (or confinement effects [1]) to differ from $T_C = 0$. Incidentally, these calculated T_C values are in reasonable agreement with available data or estimated values by other methods [22, 28, 30–32].

4. Spin wave excitations in finite ferromagnetic spin arrays

We consider a system of N interacting spins described by the following spin Hamiltonian:

$$H = -\frac{1}{2}\sum_{\langle i,j\rangle}\left[J_{ij}^{z}S_i^zS_j^z + 2J_{ij}^{\perp}\left(S_i^+S_j^- + S_i^-S_j^+\right)\right] - D\sum_i\left(S_i^z\right)^2 + g\mu_B B\sum_i S_i^z, \tag{1}$$

where $J_{ij}^{z} \geqslant 0$ represents the exchange coupling of the longitudinal component z between spins i and j, $J_{ij}^{\perp}$ is the exchange coupling on the perpendicular plane, and thus, $\lambda_{ij} = J_{ij}^{z} - J_{ij}^{\perp}$ corresponds to the anisotropic exchange between the pair of spins (i,j). In addition, D is the uniaxial magnetic anisotropy ($D > 0$ conforms with an easy axis magnetic anisotropy). The operators S_j^z and $S_j^{\pm}$ correspond to the z-component of the j-spin operator and the corresponding ladder operators $S_j^{\pm} = S_j^x \pm iS_j^y$. Here the sum over indices $\langle i,j\rangle$ denotes the sum over the first neighbors. This Hamiltonian can represent either a one-dimensional or a multidimensional system. For one-dimensional rings of finite size with N spins, we impose periodic boundary conditions where $\mathbf{S}_1 = \mathbf{S}_N$.

For the description of the spin waves, it is convenient to introduce the Fourier transforms of the exchange interaction

$$J^{z/\perp}(\mathbf{q}) = \sum_j J_{kj}^{z/\perp}e^{i\mathbf{q}\cdot\left(\mathbf{R}_j-\mathbf{R}_k\right)}, \tag{2}$$

where we have assumed that the local $\mathbf{S}_j$-spin is at the $\mathbf{R}_j$ position, and the dimensionless parameter

$$\xi = J^{\perp}(\mathbf{q})/J^{z}(\mathbf{q}) = J_{k,j}^{\perp}/J_{k,j}^{z}, \quad \forall j,k. \tag{3}$$

Notice that the periodicity of the lattice implies that $J^{z/\perp}(\mathbf{q})$ does not depend on the k-lattice site. For simplicity, we assume that all spins are of equal magnitude $S \geqslant 1/2$ and a uniform exchange interaction between first-neighbors, i.e. $J_{kj}^{z/\perp} = J^{z/\perp}$ if j and k are first-neighbors and zero otherwise.

The ground state $|G\rangle$ of Hamiltonian (1) for J^z, $J^{\perp} > 0$ corresponds to the Weiss state that can be written as $|G\rangle = \prod_{i=1}^{N}|-S\rangle$[6]. For finite-size systems, one can in principle solve Hamiltonian (1) and find the discrete energy levels ϵ_n and the corresponding eigenvectors $|\epsilon_n\rangle$. These states can be written in terms of the spin configurations $|\alpha\rangle \equiv |m_1, m_2, \ldots, m_N\rangle$, where m_i is the spin quantum number associated with S_i^z. Then, we can write the eigenvectors of H as $|\epsilon_n\rangle = \sum_\alpha \langle\alpha|\epsilon_n\rangle|\alpha\rangle$.

4.1. Single-spin excitation

Single magnons are delocalized spin waves whose total spin differs in one unit of angular momentum with respect to the ground state of the magnet. In our finite-size system described by equation (1), we define the normalized local excitation of the ℓ spin of the Weiss state as

$$|\ell\rangle = \frac{1}{\sqrt{2S}}S_\ell^+|G\rangle. \tag{4}$$

Here we have included the normalization factors similarly to what is done in usual semiclassical spin-wave theory for extended systems with the magnon momentum q a continuous variable (see supporting information for further details). In our case, a finite-size spin wave-like state containing a single magnon has the form

$$|\mathbf{q}\rangle = \frac{1}{\sqrt{N}}\sum_{\ell=1}^{N}e^{i\mathbf{q}\cdot\mathbf{R}_\ell}|\ell\rangle, \tag{5}$$

with $\mathbf{R}_\ell$ the position of the ℓ-spin. Notice that, for a closed one-dimensional chain, the momentum q is quantized due to the periodic boundary conditions (see supplementary material). Thus, we can define the overlap of the eigenvectors of our spin Hamiltonian with the $|\mathbf{q}\rangle$ spin wave as

$$\psi_{\mathbf{q}}^{n} \equiv \langle\mathbf{q}|\epsilon_n\rangle = \frac{1}{\sqrt{N}}\sum_\ell e^{-i\mathbf{q}\cdot\mathbf{R}_\ell}\sum_\alpha\langle\ell|\alpha\rangle\langle\alpha|\epsilon_n\rangle, \tag{6}$$

[6] The degeneracy of the ground state level could be broken by an infinitesimal applied field $B_z > 0$, in which case the $S_z = -S$ projection is favored.

where one finds that

$$\langle \ell|\alpha\rangle \equiv \frac{1}{\sqrt{2S}}\langle G|S_\ell^-|m_1,\ldots,m_N\rangle = \delta_{m_1,-S}\ldots\delta_{m_\ell-1,-S}\delta_{m_\ell,-S+1}\delta_{m_\ell+1,-S}\ldots\delta_{m_N,-S}. \tag{7}$$

The excitation energy of a single spin wave can be found from semiclassical arguments and it reads as [2]:

$$E_{\rm SW}(\mathbf{q}) = S\left(J^\perp(\mathbf{0})/\xi - J^\perp(\mathbf{q})\right) + D(2S-1) + g\mu_B B, \tag{8}$$

where $\xi = J^\perp(\mathbf{q})/J^z(\mathbf{q})$. Hence, the spin-wave spectrum presents an energy gap of magnitude $S\left(J^\perp(\mathbf{0})/\xi - J^\perp(\mathbf{0})\right) + D(2S-1)$ at zero magnetic field. In finite-size systems, the momentum $\mathbf{q}$ is quantized into a set of discrete values $\{\mathbf{q}_i\}$ and, thus, for each energy level ϵ_n there will be a given number $\mathcal{N}_n$ of states with overlaps $\psi^n_{\mathbf{q}_i}$ above a given threshold ε. Moreover, when finite-size effects are negligible, not only does the lowest energy ϵ_n reproduce the spin-wave dispersion $E_{\rm SW}(\mathbf{q})$ perfectly [47] but, as we shall see below, it leads to a single state with non-negligible overlap for $E_{\rm SW}(\mathbf{q}_i) = \epsilon_n$. Next, we consider the two-magnon excitations, which is somewhat more involved but it is exactly solvable, as shown by Tonegawa [48].

4.2. Two-spin excitation

Two-magnon excitations of a ferromagnet correspond to spin waves differing by two units of angular momentum from the totally aligned states, a set of states that comprises an invariant subspace under the dynamical motion defined by the Heisenberg Hamiltonian [49]. These two-magnon excitations depend on the momentum of the pair of magnons $\mathbf{k}_1$ and $\mathbf{k}_2$ or, alternatively, on the total momentum $\mathbf{Q}$ and the difference $\mathbf{q}$, where $\mathbf{k_1} = \mathbf{Q}/2 + \mathbf{q}$ and $\mathbf{k_2} = \mathbf{Q}/2 - \mathbf{q}$. It embraces a continuum of states corresponding to two non-interacting magnons. In addition, there may be up to two branches below the continuum that correspond to two-magnon bound states resulting from the magnon-magnon interaction that confines both magnons together [49].

Two-magnon excitations are essential to understand the low-temperature Raman scattering ($\mathbf{Q} = \mathbf{0}$) where they manifest as resonances close to the bound states energies [50], the enhanced relaxation of uniform modes observed in FMR [16], or the strongly temperature-dependent peaks in neutron scattering [51–53]. Moreover, exchange Hamiltonians like (1) display two-magnon bound states bellow a two-magnon continuum [54, 55]. These multiple-magnon bound states can be detected in the resonant spectra [56, 57] or in electron spin resonance experiments [58], with intensities that decrease exponentially upon lowering the temperature or increasing the multiplicity of the magnon mode. However, due to the dominant statistical weight of the two-magnon continuum in thermodynamic measurements, and the common forbidden transition character of the $\mathbf{Q} = \mathbf{0}$ point explored in most spectroscopic techniques [58], the inherently weak intensity of the two-magnon cross-section makes the observation of these bound states quite challenging. Nevertheless, they can play an important role in the entanglement and non-equilibrium dynamics as explicitly demonstrated in trapped-ions quantum simulators [59, 60].

The problem of the two magnons has been solved exactly by Tonegawa [48] in one and two dimensions (the main results can be found in the supplementary material). He found that there are two branches of the energy of the two-magnon bound state $E_{\rm 2M}(\mathbf{Q})$. He observed that below a certain threshold momentum $\rm Q_{th}$, there is a pair of complex conjugate solutions and one real solution. This indicates that the corresponding bound-state branch is no longer stable and the bound-state dispersion crosses the continuum. Moreover, for certain regions of the parameter space, negative values of the (excitation) energy of the two-magnon-bound state can be obtained. This reflects that one-dimensional ferromagnets may show unstable fully aligned states along the quantization axis z even for parameters for which the single magnon excitation energy is positive. In addition, it is possible to find single-magnon energies $E_{\rm SW}(\mathbf{q})$ above the two-magnon bound states $E_{\rm 2M}(Q)$.

In particular, he found that the amplitude $\psi_Q(\ell,\ell')$ for finding two spin-deviations at the ℓth and ℓ'th sites decays quite fast with $|\ell-\ell'|$, with $\psi_Q(\ell,\ell') = \delta_{\ell,\ell'}$ at the Brillouin zone boundary for one of the two energy branches, the so-called *Ising type*, while $\psi_Q(\ell,\ell') = \delta_{\ell',\ell+1}$ for the second one, called as *Bethe type*. For an arbitrary value of $\mathbf{Q}$, one of the two magnon bound states has a larger amplitude on nearest neighbors while the second one has a larger amplitude on the same site, but they can not be classified rigorously into either type [48]. In the same way, the amplitudes $\psi_Q(\ell,\ell')$ decay much slower with $|\ell-\ell'|$ as we move away from the first Brillouin zone boundaries.

Let us formulate the problem using the ideas of spin-wave theory. The normalized two-spin excitation corresponding to sites ℓ and ℓ' is defined as

$$|\ell,\ell'\rangle = \chi^S_{\ell\ell'} S^+_\ell S^+_{\ell'}|G\rangle, \tag{9}$$

Table 2. Values of the spin S, relative local magnetic anisotropy D/J and anisotropic exchange $(J^z - J)/J$ for four different spin rings whose parameters resemble those of Co/Pt, CrI_3, Fe-DCA/Au and $MnBi_2Te_4$, respectively. For simplicity, we have denoted $J^\perp = J$.

System	S	D/J	$(J^z - J)/J$
A	1	0.02	−0.003
B	3/2	0.01	0.04
C	2	0.25	−0.03
D	5/2	0.26	−0.03

where $\chi^S_{\ell\ell'} = 1/2S$ if $\ell \neq \ell'$ and $\chi^S_{\ell\ell} = 1/\sqrt{4S(2S-1)}$. Similarly to the single spin excitations, we can define a two-magnon wave function as

$$|\mathbf{Q},\mathbf{q}\rangle = \frac{1}{\sqrt{N}} \sum_{\ell,\ell'} e^{i\mathbf{Q}\cdot(\mathbf{R}_\ell + \mathbf{R}_{\ell'})} e^{i\mathbf{q}\cdot(\mathbf{R}_\ell - \mathbf{R}_{\ell'})} b_{|\ell-\ell'|} |\ell,\ell'\rangle, \tag{10}$$

where the normalization condition imposes that $\sum_{\ell\ell'} \left| b_{|\ell-\ell'|} \right| = N$. We now define the overlaps of the eigenvectors $|\epsilon_n\rangle$ with the two-magnon waves

$$\begin{aligned} \psi^{\text{Bethe}}_{\mathbf{Q},\mathbf{q}}(n) &\equiv \frac{1}{\sqrt{N}} \sum_{\ell} \sum_{n.n.,\ell} e^{-i\mathbf{Q}\cdot(\mathbf{R}_\ell + \mathbf{R}_{n.n.,\ell})} e^{-i\mathbf{q}\cdot(\mathbf{R}_\ell - \mathbf{R}_{n.n.,\ell})} \sum_{\alpha} \langle \ell, n.n.|\alpha\rangle\langle\alpha|\epsilon_n\rangle \\ \psi^{\text{Ising}}_{\mathbf{Q}}(n) &\equiv \frac{1}{\sqrt{N}} \sum_{\ell} e^{-2i\mathbf{Q}\cdot\mathbf{R}_\ell} \sum_{\alpha} \langle \ell,\ell|\alpha\rangle\langle\alpha|\epsilon_n\rangle, \end{aligned} \tag{11}$$

where $n.n.,\ell$ indicates that the sum is realized over the nearest neighbors of spin ℓ. Markedly, while for the Ising-type the two-magnon is fully defined by a total momentum $\mathbf{Q}$, the Bethe-type two-magnon state also depends on the momentum difference $\mathbf{q}$ and so does also the overlap $\psi^{\text{Bethe}}_{\mathbf{Q},\mathbf{q}}(n)$. These overlaps contain, in addition to the two-magnon bound state contribution, a portion of two unbound magnons that, in average, occupy either the same or neighboring sites for each type, respectively [60].

As it happens for the single magnon, for each energy level ϵ_n, there will be a finite number of states with overlaps $\psi^n_{\mathbf{Q},\mathbf{q}}$ above a given threshold.

4.3. Results for a one-dimensional toy model

To further extend our understanding of the spin waves and their connection with the magnetic anisotropy, we will analyze the energy spectrum of a closed finite ring of anisotropic spins. We stress that, from a practical point of view, the main effect of the change in dimensionality is to restrict the sums in equations (1) and (2) over the first neighbors. For the ring with N spins, the momentum q of the spin waves is quantized, i.e. $q_n = 2\pi n/(aN)$, $n = 0,\ldots,N-1$, where a is the distance between spins in the chain. Here, we have considered four scenarios that mimic the properties of the systems studied in section 2. The model parameters of each of these systems are summarized in table 2. The four cases A-D correspond to situations of increasing anisotropy, starting from the almost isotropic Heisenberg-like $S = 1$ chain in A and finishing with the largest anisotropy-induced gap for case D.

Figure 2 summarizes the main results of the spin waves in close rings with the parameters of table 2. The single spin wave solution $E_{\text{SW}}(q)$ for the extended system has been plotted as a reference for the four cases. Case A represents the closest case to the isotropic Heisenberg spin chain. As observed, it does not show any apparent gap in the spectrum of spin waves. The presence of local anisotropy $D \neq 0$ or anisotropic exchange induces a finite energy gap at $q = 0$ of magnitude $E^{\text{gap}}_{\text{SW}} = 2SJ^\perp(1/\xi - 1) + D(2S-1)$. This is clearly observed in cases C and D (notice that the gap has been scaled by JS).

Let us now analyze what happens with the projection of the energy eigenstates of (1) on the single-magnon states for finite rings. In all cases, the energy of the states that have sizeable projection with single-magnon excitations coincides exactly with the energy given by the single-magnon dispersion curve $E_{\text{SW}}(q)$ due to the preserved translational symmetry of the ring. These projections are depicted in figure 2 by the size of the corresponding symbols. Hence, the only effect of the finite size is the quantization of the momentum q.

As explained in section 4.2, two-magnon excitations can be relevant in the dynamics of these spin systems, specially in the low-temperature limit. With this idea in mind, we have also explored the two-magnon excitations of the above systems. The results are shown in figure 3, where we have included as a reference both the single-magnon $E^{\text{ring}}_{\text{SW}}(Q)$ and two-magnon bound state dispersion $E_{2\text{M}}(Q)$ curves, as well as the two-magnon continuum $E_{2\text{SW}}(Q,q)$ of the extended systems. The calculated energy eigenvalues of the finite rings and their projections, $\psi^{\text{Bethe}}_{Q,0}(n)$ and $\psi^{\text{Ising}}_{Q}(n)$, are depicted by the triangles and squares,

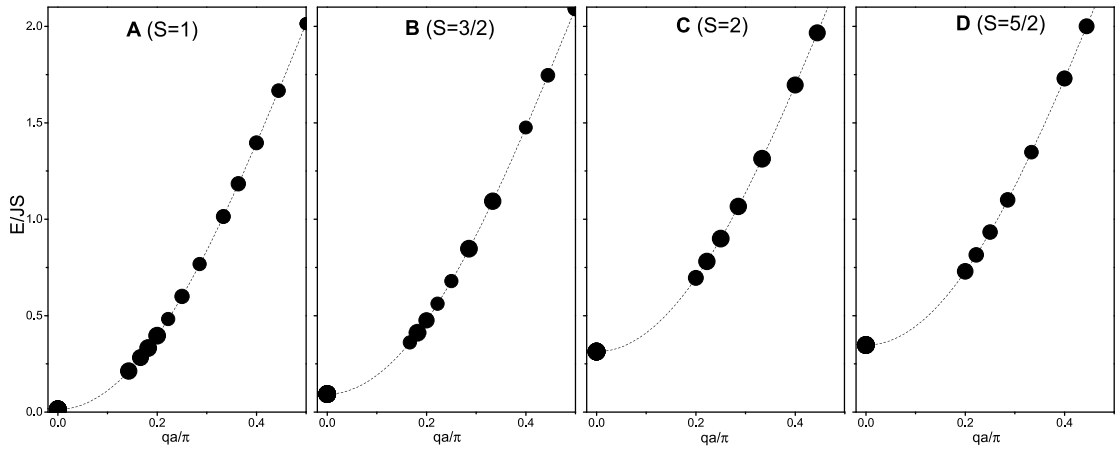

Figure 2. Single magnon excitations of finite-size rings. Single-magnon energies (dashed lines) as calculated from $E_{\mathrm{SW}}(q)$ and from the diagonalization of the finite-size Hamiltonian (1) for a one-dimensional ring (black circles) corresponding to A, B, C, and D systems in table 2. Each non-zero momentum $q = 2\pi n/(Na)$ is associated with a single chain of size N. The symbol's sizes are proportional to the weights ψ_q^n for the single magnon, and only states with projections ψ_q^n above a threshold value of $\epsilon = 0.1$ have been depicted.

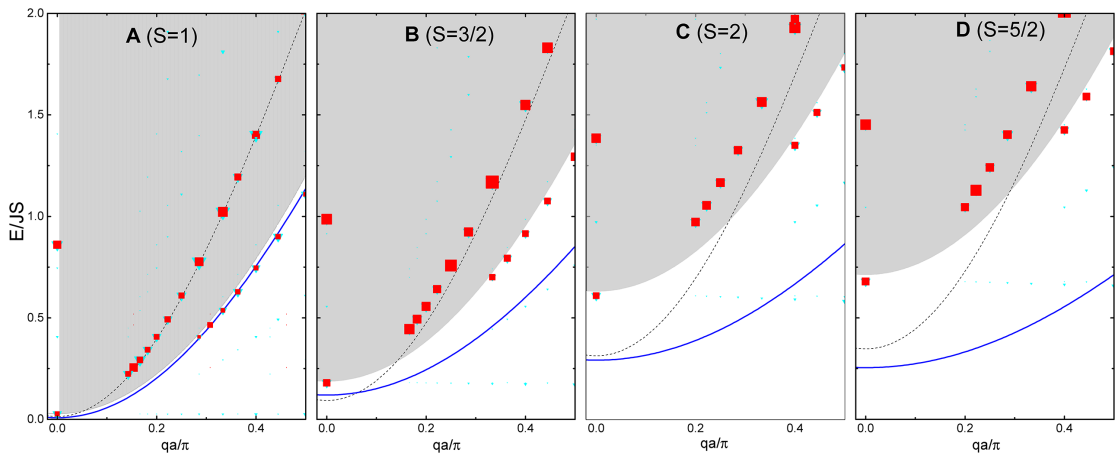

Figure 3. Two-magnon spectra for systems A–D. The shaded area represents the two-magnon continuum $E_{2\mathrm{SW}}$, while the blue solid line corresponds to the two-magnon bound state energy $E_{2\mathrm{M}}(Q)$. The symbols represent the energies ϵ_n from the exact diagonalization of Hamiltonian (1) of N spins and the corresponding weights $\psi_{Q,0}^{\mathrm{Bethe}}(n)$ for the Bethe-type (cyan triangles), and $\psi_Q^{\mathrm{Ising}}(n)$ for the Ising-type (red squares) two-magnon spin waves (only weights above 0.1 have been represented). The symbol's sizes are proportional to the weights. The single magnon solution $E_{\mathrm{SW}}(Q)$ (dashed line) has been added as a reference. Each non-zero momentum $Q = 2\pi n/(Na)$ is associated with a single chain size N.

respectively [see supplementary material for detailed expressions of continuum $E_{2\mathrm{SW}}(Q, q)$ and bound-states energies $E_{2\mathrm{M}}(Q)$]. For the parameters in A–D, only one of the solutions corresponding to the bound states is positive and real. Notice that the two-magnon bound state energies constitute a lower bound to the energy of the continuum, and though the bound state energies approach the bottom of the continuum as $Q \to 0$, it may or may not merge with it [48, 61].

Concerning the dispersion curves, we observe that in the long wave length limit, the two magnon dispersion curve can cross the single magnon curve (case B). Interestingly, not only an energy gap can also be opened in the two-magnon-bound states' excitations, but it can lay either above (as in B) or below (C and D) the single-magnon excitation, a situation typically found for large enough anisotropy D, and where a large impact of two-magnon excitations is expected [48]. Indeed, Tonegawa [48] argued that this situation indicates that the states in which all the spins aligned along the z-axis are unstable.

Let us focus now on the projection of the energy eigenstates of (1) on the two-magnon states for finite rings. To facilitate the interpretation, only the $N = 10$ energies ϵ_n have been depicted for $q = 0$, the only case where the different chain sizes correspond to the same momentum. In the long wavelength limit, the lowest excitation energy appears right below the two-magnon continuum (shaded area in the figure). Furthermore, as advanced in section 4.2, the overlaps defined in equation (11) contain a contribution of single-magnon

character whose energy matches the single-magnon dispersion curve for almost isotropic rings (case A), clearly reflected in figure 3. Additionally, there exist other states with the two-magnon-bound state character that follow the energy of the two-magnon bound state dispersion curve for arbitrary momentum, showing both Ising- and Bethe-like character in the low-q region.

The situation changes quite drastically when anisotropy is included [cases B, C, and D]. First, the quantized two-magnon excitation energies deviate appreciably from the dispersion curves of the infinite lattice. In particular, the contribution that in case A followed the energy of the single-magnon semiclassical solution now appears at higher energies, well within the two-magnon continuum, and having a prominent Ising-type character (red squares in the figure). This is especially visible in cases C and D, although it can also be noticed in case B. Second, the two-magnon bound state component of the projections, which for the isotropic case almost overlaps with the solution depicted with the blue curve in the figure (see case A), now also moves upwards in energy (cases B–D) when anisotropy increases. Finally, contrary to the single magnon case where there is a single eigenstate of H that does overlap with the spin wave solution and, hence, has a well-defined character, now a large number of eigenstates with both Ising- and Bethe-type characters display finite but small overlap with the two-magnon sates (10).

5. Summary and conclusions

Here, we have estimated the Curie temperatures of different two-dimensional materials based on the simple phenomenological expressions provided by Torelli and Olsen [42]. In so doing, the isotropic and anisotropic exchange coupling constants, as well as the single-ion anisotropy, are obtained by mapping the total energy differences obtained from DFT calculations for different spin configurations with a spin Hamiltonian model.

Later on, in order to explore the low-energy magnetic excitations in systems with magnetic anisotropy, we use a simple finite-size periodic chain model of spin Hamiltonian with the previously calculated exchange coupling constants and anisotropy. The corresponding eingenstates are found by exact diagonalization. Their projection onto single-magnon and two-magnon states reveals important changes in the spin wave excitation spectrum for large values of the magnetic anisotropy, both single-ion and anisotropic exchange. We not only reproduce the well-known opening of a gap in the single-magnon excitations, but also find the importance of two-magnon excitations in the low-energy spin wave excitation spectrum. In addition, two-magnon excitations of different kinds, including two-magnon bound states [62], are found. These results suggest that some of the two-dimensional materials considered in this work, particularly those with large magnetic anisotropy, may present a low energy spin excitation spectrum that differs significantly from the one determined by a gapless semiclassical single magnon dispersion curve. Therefore, we speculate that, in systems with large magnetic anisotropy, multi-magnon processes can play an important role in determining the low-energy magnetic excitations, although the intensity of the corresponding signal is expected to be weaker [63] and, thus, are relevant in the interpretation of the low-temperature properties of these two-dimensional ferromagnets. Its confirmation, of course, requires the use of precise and sensitive techniques, like Raman scattering [22] or FMR [15–17].

Data availability statement

All data that support the findings of this study are included within the article (and any supplementary files).

Acknowledgments

We are grateful to Nicolas Lorente and Leonid M. Sandratskii for fruitful discussions. This work was supported by MCIN/ AEI /10.13039/ 501100011033/ (Grants PID2022-138269NB-I00, PID2019-103910GB-I00, PID2022-137685NB-I00, and PID2022-138210NB-I00), and FEDER 'Una manera de hacer Europa'. We also acknowledge the support by the University of the Basque Country (Grant No. IT1527-22) as well as MCIN with funding from European Union NextGenerationEU (PRTR-C17.I1) promoted by the Government of Aragon.

ORCID iDs

Fernando Delgado https://orcid.org/0000-0003-2180-5273
Mikhail M Otrokov https://orcid.org/0000-0001-5775-3386

References

[1] Jenkins S *et al* 2022 Breaking through the Mermin-Wagner limit in 2D van der Waals magnets *Nat. Commun.* **13** 6917
[2] Majlis N 2007 *Quantum Theory Of Magnetism* (World Scientific Publishing Company)
[3] Abragam A and Bleaney B 1970 *Electron Paramagnetic Resonance of Transition Ions* (Oxford University Press)
[4] Wang Q H *et al* 2022 The magnetic genome of two-dimensional van der Waals materials *ACS Nano* **16** 6960–7079
[5] Stöhr J 1995 x-ray magnetic circular dichroism spectroscopy of transition metal thin films *J. Electron Spectrosc. Relat. Phenom.* **75** 253–72
[6] Amemiya K *et al* 2004 Direct observation of magnetic depth profiles of thin Fe films on Cu(100) and Ni/Cu(100) with the depth-resolved x-ray magnetic circular dichroism *Appl. Phys. Lett.* **84** 936–8
[7] Sakamaki M and Amemiya K 2017 Nanometer-resolution depth-resolved measurement of florescence-yield soft x-ray absorption spectroscopy for FeCo thin film *Rev. Sci. Instrum.* **88** 083901
[8] Majkrzak C *et al* 2005 *Polarized Neutron Reflectometry* (Elsevier)
[9] Callori S J *et al* 2020 Using polarized neutron reflectometry to resolve effects of light elements and ion exposure on magnetization *Solid State Physics* vol 71, ed R L Stamps (Academic) ch 3, pp 73–116
[10] Vettoliere A *et al* 2023 Superconducting quantum magnetic sensing *Quantum Materials, Devices and Applications* ed M Henini and M O Rodrigues (Elsevier) ch 3, pp 43–85
[11] Fleury P A and Guggenheim H J 1970 Magnon-pair modes in two dimensions *Phys. Rev. Lett.* **24** 1346–9
[12] Devereaux T P and Hackl R 2007 Inelastic light scattering from correlated electrons *Rev. Mod. Phys.* **79** 175–233
[13] Minh Hien N T *et al* 2010 Raman scattering studies of the magnetic ordering in hexagonal $HoMnO_3$ thin films *J. Raman Spectrosc.* **41** 983–8
[14] Zhang Y *et al* 2020 Magnetic order-induced polarization anomaly of Raman scattering in 2D magnet CrI_3 *Nano Lett.* **20** 729–34
[15] Kittel C 1948 On the theory of ferromagnetic resonance absorption *Phys. Rev.* **73** 155–61
[16] Beaujour J-M *et al* 2009 Ferromagnetic resonance linewidth in ultrathin films with perpendicular magnetic anisotropy *Phys. Rev.* B **80** 180415
[17] Usov N 2019 Ferromagnetic resonance in thin ferromagnetic film with surface anisotropy *J. Magn. Magn. Mater.* **474** 118–21
[18] Wiesendanger R 2009 Spin mapping at the nanoscale and atomic scale *Rev. Mod. Phys.* **81** 1495–550
[19] Klein D R *et al* 2018 Probing magnetism in 2D van der Waals crystalline insulators via electron tunneling *Science* **360** 1218–22
[20] Gao C L *et al* 2008 Spin wave dispersion on the nanometer scale *Phys. Rev. Lett.* **101** 167201
[21] Balashov T *et al* 2006 Magnon excitation with spin-polarized scanning tunneling microscopy *Phys. Rev. Lett.* **97** 187201
[22] Cenker J *et al* 2021 Direct observation of two-dimensional magnons in atomically thin CrI_3 *Nat. Phys.* **17** 20–25
[23] Chen L *et al* 2021 Magnetic field effect on topological spin excitations in CrI_3 *Phys. Rev.* X **11** 031047
[24] Olsen T 2021 Unified treatment of magnons and excitons in monolayer CrI_3 from many-body perturbation theory *Phys. Rev. Lett.* **127** 166402
[25] Soenen M *et al* 2023 Stacking-dependent topological magnons in bilayer CrI_3 *Phys. Rev. Mater.* **7** 024421
[26] Soenen M and Milošević M V 2023 Tunable magnon topology in monolayer CrI_3 under external stimuli *Phys. Rev. Mater.* **7** 084402
[27] Šabani D *et al* 2020 *Abinitio* methodology for magnetic exchange parameters: generic four-state energy mapping onto a Heisenberg spin Hamiltonian *Phys. Rev.* B **102** 014457
[28] Otrokov M M *et al* 2019 Unique thickness-dependent properties of the van der Waals interlayer antiferromagnet $MnBi_2Te_4$ films *Phys. Rev. Lett.* **122** 107202
[29] Otrokov M M *et al* 2019 Prediction and observation of an antiferromagnetic topological insulator *Nature* **576** 416–22
[30] Huang B *et al* 2017 Layer-dependent ferromagnetism in a van der Waals crystal down to the monolayer limit *Nature* **546** 270–3
[31] Lobo-Checa J *et al* 2024 Ferromagnetism on an atom-thick & extended 2d metal-organic coordination network *Nat. Commun.* **15** 1858
[32] Zimmermann B *et al* 2019 Comparison of first-principles methods to extract magnetic parameters in ultrathin films: Co/Pt(111) *Phys. Rev.* B **99** 214426
[33] Lado J L and Fernández-Rossier J 2017 On the origin of magnetic anisotropy in two dimensional CrI_3 *2D Mater.* **4** 035002
[34] Soriano D *et al* 2020 Magnetic two-dimensional chromium trihalides: a theoretical perspective *Nano Lett.* **20** 6225–34
[35] Blöchl P E 1994 Projector augmented-wave method *Phys. Rev.* B **50** 17953
[36] Kresse G and Furthmüller J 1996 Efficient iterative schemes for *ab initio* total-energy calculations using a plane-wave basis set *Phys. Rev.* B **54** 11169
[37] Kresse G and Joubert D 1999 From ultrasoft pseudopotentials to the projector augmented-wave method *Phys. Rev.* B **59** 1758
[38] Kresse G and Hafner J 1993 *Ab initio* molecular dynamics for liquid metals *Phys. Rev.* B **47** 558–61
[39] Perdew J P *et al* 1996 Generalized gradient approximation made simple *Phys. Rev. Lett.* **77** 3865–8
[40] Anisimov V I *et al* 1991 Band theory and mott insulators: Hubbard *U* instead of Stoner *I Phys. Rev.* B **44** 943–54
[41] Dudarev S L *et al* 1998 Electron-energy-loss spectra and the structural stability of nickel oxide: an LSDA+U study *Phys. Rev.* B **57** 1505–9
[42] Torelli D and Olsen T 2018 Calculating critical temperatures for ferromagnetic order in two-dimensional materials *2D Mater.* **6** 015028
[43] He X *et al* 2021 Tb2j: a python package for computing magnetic interaction parameters *Comput. Phys. Commun.* **264** 107938
[44] Liao J-J *et al* 2023 Spin reorientation and Curie temperature promotion in CrI_3 - Bi van der Waals heterostructures *Phys. Rev.* B **107** 184403
[45] Simon E *et al* 2018 Magnetism of a Co monolayer on Pt(111) capped by overlayers of 5*d* elements: a spin-model study *Phys. Rev.* B **97** 134405
[46] Yosida K 2001 *Theory of Magnetism (Springer Series in Solid-State Sciences)* (Springer)
[47] Gauyacq J P and Lorente N 2011 Excitation of spin waves by tunneling electrons in ferromagnetic and antiferromagnetic spin-1/2 Heisenberg chains *Phys. Rev.* B **83** 035418
[48] Tonegawa T 1970 Two-magnon bound states in the Heisenberg ferromagnet with anisotropic exchange and uniaxial anisotropy energies *Prog. Theor. Phys. Suppl.* **46** 61–83
[49] Bethe H 1931 Zur theorie der metalle: I. eigenwerte und eigenfunktionen der linearen atomkette *Z. Phys.* **71** 205–26
[50] Loly P D and Choudhury B J 1976 Two-magnon spectra and ising anisotropy: The relationship between resonances and bound states *Phys. Rev.* B **13** 4019–28
[51] Cowley R A *et al* 1969 Two-magnon scattering of neutrons *Phys. Rev. Lett.* **23** 86–89

[52] Huberman T et al 2005 Two-magnon excitations observed by neutron scattering in the two-dimensional spin-5/2 Heisenberg antiferromagnet Rb_2MnF_4 Phys. Rev. B 72 014413
[53] Körner M et al 2013 Two-magnon scattering in permalloy thin films due to rippled substrates Phys. Rev. B 88 054405
[54] Hanus J 1963 Bound states in the Heisenberg ferromagnet Phys. Rev. Lett. 11 336–8
[55] Wortis M 1963 Bound states of two spin waves in the Heisenberg ferromagnet Phys. Rev. 132 85–97
[56] Date M and Motokawa M 1966 Spin-cluster resonance in $CoCl_2.2H_2O$ Phys. Rev. Lett. 16 1111–4
[57] Torrance J B and Tinkham M 1969 Excitation of multiple-magnon bound states in $CoCl_2.2H_2O$ Phys. Rev. 187 595–606
[58] Hoogerbeets R et al 1984 Evidence for magnon bound-state excitations in the quantum chain system $(C_6H_{11}N_3)CuCl_3$ J. Phys. C: Solid State Phys. 17 2595
[59] Fukuhara T et al 2013 Microscopic observation of magnon bound states and their dynamics Nature 502 76–79
[60] Kranzl F et al 2023 Observation of magnon bound states in the long-range, anisotropic Heisenberg model Phys. Rev. X 13 031017
[61] Sharma P et al 2022 Multimagnon dynamics and thermalization in the $S = 1$ easy-axis ferromagnetic chain Phys. Rev. B 105 054413
[62] Silberglitt R and Torrance J B 1970 Effect of single-ion anisotropy on two-spin-wave bound state in a Heisenberg ferromagnet Phys. Rev. B 2 772–8
[63] Elnaggar H et al 2023 Magnetic excitations beyond the single- and double-magnons Nat. Commun. 14 2749